SCIENCE CHINA
Physics, Mechanics & Astronomy

•Article•
Special Topic: Superconductivity and Magnetism in Transition-Metal Compounds

December 2018 Vol. 61 No. 12: 127406
https://doi.org/10.1007/s11433-018-9280-6

Thermally activated flux flow, vortex-glass phase transition and the mixed-state Hall effect in 112-type iron pnictide superconductors

XiangZhuo Xing[1], ZhanFeng Li[1], XiaoLei Yi[1], JiaJia Feng[1], ChunQiang Xu[1,2], Nan Zhou[1], Yan Meng[1], YuFeng Zhang[1], YongQiang Pan[1], LingYao Qin[1], Wei Zhou[2], HaiJun Zhao[1], and ZhiXiang Shi[1*]

[1] *School of Physics and Key Laboratory of MEMS of the Ministry of Education, Southeast University, Nanjing 211189, China;*
[2] *Advanced Functional Materials Lab and Department of Physics, Changshu Institute of Technology, Changshu 215500, China*

Received June 26, 2018; accepted July 20, 2018; published online September 11, 2018

The transport properties in the mixed state of high-quality $Ca_{0.8}La_{0.2}Fe_{0.98}Co_{0.02}As_2$ single crystal, a newly discovered 112-type iron pnictide superconductor, are comprehensively studied by magneto-resistivity measurement. The field-dependent activation energy, U_0, is derived in the framework of thermally activated flux flow (TAFF) theory, yielding a power law dependence $U_0 \sim H^{\alpha}$ with a crossover at a magnetic field around 2 T in both $H \perp ab$ and $H // ab$, which is ascribed to the different pinning mechanisms. Moreover, we have clearly observed the vortex phase transition from vortex-glass to vortex-liquid according to the vortex-glass model, and vortex phase diagrams are constructed for both $H \perp ab$ and $H // ab$. Finally, the results of mixed-state Hall effect show that no sign reversal of transverse resistivity $\rho_{xy}(H)$ is detected, indicating that the Hall component arising from the vortex flow is also negative based on the time dependent Ginzburg-Landau (TDGL) theory. Meanwhile, the transverse resistivity $\rho_{xy}(H)$ and the longitudinal resistivity $\rho_{xx}(H)$ follow the relation $|\rho_{xy}(H)| = A\rho_{xx}(H)^{\beta}$ well with an exponent $\beta \sim 2.0$, which is in line with the results in theories or experiments previously reported on some high-T_c cuprates.

thermally activated flux flow, vortex-glass transition, mixed-state Hall effect, 112-type iron pnictide superconductors

PACS number(s): 74.25.-q, 74.25.Fy, 74.25.Op, 74.25.Qt

Citation: X. Z. Xing, Z. F. Li, X. L. Yi, J. J. Feng, C. Q. Xu, N. Zhou, Y. Meng, Y. F. Zhang, Y. Q. Pan, L. Y. Qin, W. Zhou, H. J. Zhao, and Z. X. Shi. Thermally activated flux flow, vortex-glass phase transition and the mixed-state Hall effect in 112-type iron pnictide superconductors, Sci. China-Phys. Mech. Astron. **61**, 127406 (2018), https://doi.org/10.1007/s11433-018-9280-6

1 Introduction

Investigations of vortex physics for high-T_c superconductors are important both from superconducting mechanisms and potential application point of view. Vortex properties of iron-based superconductors (IBSs) have attracted a lot of interest since the discovery of superconductivity in LaFeAs(O,F) [1], and rich vortex phenomena were detected in the mixed state [2-8]. Similar to high-T_c cuprates, due to rather high T_c and small coherence length, most classes of IBSs also show strong thermal fluctuations. Generally, thermal fluctuations directly affect the vortex motion in the mixed state by the thermally activated flux flow (TAFF), which leads to large broadening of the resistive transition and a tailing-off behavior near the completion in magnetic fields [2,9-12]. The thermal activation behavior of vortices in superconductors determines their magneto-transport properties, which are critical for practical applications. Meanwhile, under the influence of strong thermal fluctuations, the vortex lattice transforms into vortex-glass state and will further transform

*Corresponding author (email: zxshi@seu.edu.cn)

to a liquid state, and disappear at $H > H_{c2}$, where H_{c2} is the upper critical field [2,4,9,10,13-15]. Depending on the type and strength of the disorder, different types of vortex-glass state can be obtained below the glass temperature, T_g [16]. Vortex-glass state has been experimentally demonstrated in IBSs, such as $BaFe_2As_2$ system [4,14,15], (Li,Fe)OHFeSe [10], $Li_x(NH_3)_yFe_2(Te_zSe_{1-z})_2$ [9] and $SmFeAsO_{0.85}$ [2], etc. On the other hand, the Hall effect in the mixed state has intimate connections with the vortex dynamics. In the mixed state of a type-II superconductor, flux motion driven by Lorentz force (perpendicular to the transport current density j) generates a dissipative fields ($E//j$) based on the Josephson's relation $E=-V_L\times B$, where V_L is the velocity of vortex motion and B is the magnetic induction [17]. Also, the vortex motion along the direction of transport current will result in the Hall electric field ($E\perp j$, B) [17-19]. Thus, the mixed state Hall effect measurement is a useful probe of vortex dynamics. The mixed state Hall effect shows very unusual features, one of the most puzzling and controversial phenomena is the Hall sign reversal that has been observed below T_c in high-T_c cuprates and some conventional superconductors [18-27]. The sign change is not expected by the classical theories in which the Hall sign in the superconducting and normal state should be the same [28,29]. Another phenomenon is a scaling law between transverse resistivity $\rho_{xy}(H)$ and the longitudinal resistivity $\rho_{xx}(H)$ in the superconducting transition region, i.e., $|\rho_{xy}(H)|=A\rho_{xx}(H)^{\beta}$ with different values of β for different materials [21,26,30-32]. Numerous attempts have been made to interpret the Hall sign reversal and scaling behavior so far, but its microscopic origin remains controversial. IBSs provide a new platform to further enhance the understanding of the mixed state Hall effect, and examine the previous experimental and theoretical statements. However, only a limited amount of studies on the mixed state Hall effect have been explored in IBSs until now [9,33-36].

In 2013, novel 112-type IBSs were discovered based on the compound $Ca_{1-x}La_xFeAs_2$ with maximum T_c=34 K [37]. The large values of critical current density and upper critical field also suggest a promising potential for applications [6,38,39]. In contrast to other commonly IBSs that own centrosymmetric lattice, these compounds crystallize in a low-symmetry crystal structure (*Monoclinic*, space group P_{21}) with an additional metallic spacer-layer, containing one-dimensional zigzag As chains (as shown in the inset of Figure 1(a)) [37,40], which significantly increases the distance between the superconducting FeAs layers, and will affect the interlayer coupling on vortex interaction. Besides, the rather high-T_c and moderate anisotropy γ (2.3-5.4) [39] make the 112-type superconductors a proper system to study correlation in the vortex dynamics between IBSs and high-T_c cuprates. Thus, it is of interest to clarify the pinning properties,

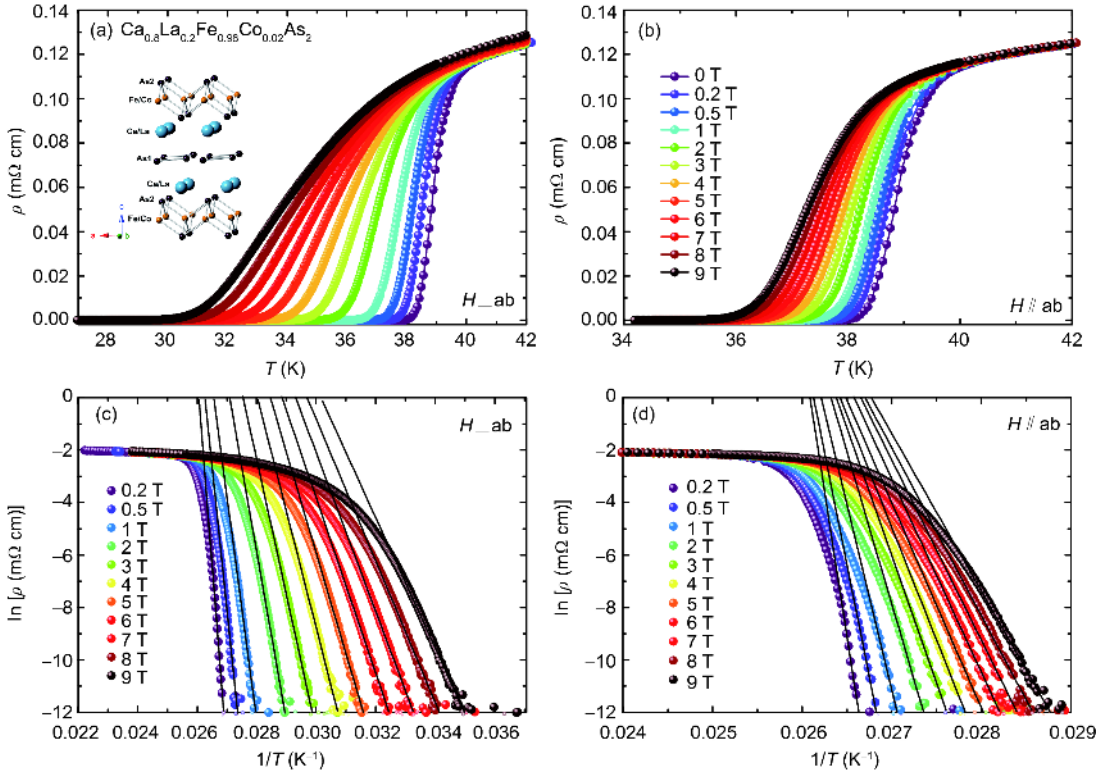

Figure 1 (Color online) Temperature dependence of the in-plane resistivities of $Ca_{0.8}La_{0.2}Fe_{0.98}Co_{0.02}As_2$ single crystal under various magnetic felds with $H\perp ab$ (a) and $H//ab$ (b). Inset of (a): crystal structure of 112-type IBSs. Arrhenius plots of the resistivities for $H\perp ab$ (c) and $H//ab$ (d). The solid lines are fitting results from the Arrhenius relation.

diverse phases and vortex dynamics, which will also be helpful for practical applications of 112-type IBSs. It is well known that the intrinsic vortex behavior of a superconductor should be studied using high-quality single crystals, since the nature of the vortex is highly sensitive to the type and density of defects. Recently, we have synthesized high-quality $Ca_{0.8}La_{0.2}Fe_{0.98}Co_{0.02}As_2$ single crystals with bulk T_c~38 K by La and small amount of Co co-doping method [38,41], avoiding the poor quality with inhomogeneity and low superconducting volume fraction commonly existed in 112-type IBSs. Benefit from the high-quality single crystals, it becomes possible to study the intrinsic vortex dynamics in 112-type IBSs.

The electrical transport measurement in the mixed state is a powerful probing technique of vortex motion. In order to gain more insight into the vortex phase and dynamic of the 112-type IBSs, in this paper, we report the vortex properties of $Ca_{0.8}La_{0.2}Fe_{0.98}Co_{0.02}As_2$ single crystal in the mixed state by magneto-resistivity measurement. It is found that the flux pinning energy shows double-linear field dependences, indicating a crossover from single vortex pinning region to collective creep pinning region with increasing field. Meanwhile, a clear phase transition from vortex-glass to vortex-liquid was confirmed based on the vortex-glass theory, and the vortex phase diagrams were constructed for both $H\perp ab$ and $H//ab$. Beside these, the Hall effect in the mixed state were also examined, and compared to previous findings in high-T_c cuprate superconductors, MgB_2 and other IBSs.

2 Experimental details

Single crystals of $Ca_{0.8}La_{0.2}Fe_{0.98}Co_{0.02}As_2$ investigated in this work were synthesized by the self-flux method. Details of the crystal growth and characterizations were described in our previous reports [38,41]. Magneto-transport measurements were carried out in a PPMS-9 T system (Quantum Design) with a standard six-probe technique. Magneto-resistivity data were extracted from the difference of the transverse resistivity measured at positive and negative fields in order to eliminate the effect of misalignment of the Hall contacts, i.e. $\rho_{xx}(\mu_0H)=[\rho(+\mu_0H)+\rho(-\mu_0H)]/2$ and $\rho_{xy}(\mu_0H)=[\rho(+\mu_0H)-\rho(-\mu_0H)]/2$.

3 Results and discussion

Figure 1(a) and (b) present the temperature dependence of resistivity in different magnetic fields for $H\perp ab$ and $H//ab$, respectively. In zero field, the sample shows a sharp superconducting transition around 38.8 K (~50%ρ_n) with transition width ΔT_c~1.1 K (90%ρ_n-10%ρ_n), indicating the high quality of our sample. With the increase of applied magnetic field, the superconducting transition gradually shifts to lower temperatures and the width becomes significantly broadened. Additionally, the tailing effect just before reaching zero resistivity at low temperatures becomes more evident with a gradual suppression of the temperature corresponding to zero resistivity. Similar phenomena, which have also been observed in many other high-T_c superconductors such as cuprates [20,42,43], (Li,Fe)OHFeSe [10], $Li_x(NH_3)_yFe_2(Te_zSe_{1-z})_2$ [9], $Tl_{0.58}Rb_{0.42}Fe_{1.72}Se_2$ [11] and 1111-type iron pnictides [2,12], are generally interpreted in terms of TAFF that is intimately linked to the thermal fluctuations. The magnitude of thermal fluctuations is quantified by the Ginzburg parameter, $G_i=[(2\pi\mu_0k_BT_c\lambda_{ab}^2(0))/(\Phi_0^2\xi_c(0))]^2/2$, where $\lambda_{ab}(0)$ is the penetration depth at 0 K for $H//ab$ and $\xi_c(0)$ is the coherence length at 0 K for $H//c$ [44]. Assuming $\lambda_{ab}(0)$=300-500 nm (The penetration depth $\lambda_{ab}(0)$ was calculated from the lower critical field H_{c1}, details of which will be published in elsewhere.) and $\xi_c(0)$=1.44 nm taken from ref. [39], G_i number is estimated to be $2\times(10^{-2}$-$10^{-3})$, this value is in a range comparable to that of cuprates and other iron pnictides, indicating that the strong thermal fluctuations is expected to be substantial in $Ca_{0.8}La_{0.2}Fe_{0.98}Co_{0.02}As_2$. According to the TAFF theory [44–46], the resistivity in TAFF region can be expressed as:

$$\rho(T,H) = (2\rho_c U/T)\exp(-U/T) = \rho_{0f}\exp(-U/T), \quad (1)$$

where U is the thermally activated energy (TAE), and the prefactor $2\rho_cU/T$ is usually assumed as a constant ρ_{0f}. Assuming $U(T,H)=U_0(H)(1-t)$, where $t=T/T_c$, then eq. (1) can be simplified to the Arrhenius relation:

$$\ln\rho(T,H) = \ln\rho_0(H) - U_0(H)/T, \quad (2)$$

where $\ln\rho_0(H) = \ln\rho_{0f} + U_0(H)/T_c$ and $U_0(H)$ is the apparent activation energy, which plays the role of effective pinning barrier. Furthermore, it can be concluded that $-\mathrm{d}\ln\rho/\mathrm{d}(1/T) = U_0(H)$. Hence $\ln\rho$ vs $1/T$ should be linear in the TAFF region. The slope is $-U_0(H)$ and its y intercept is represented by $\ln\rho_0(H)$. As shown in Figure 1(c) and (d), the resistivities as a function of $1/T$ follow an exponential dependence, as presented by the solid lines.

Figure 2 depicts the magnetic field dependence of $U_0(H)$ for $H\perp ab$ and $H//ab$, calculated from the linear slope of the Arrhenius plot. It is worth mentioning that the value of $U_0(H)$ is much larger than that deduced from the magnetic relaxation rate in our previous report [6]. This is due to a relatively low current density applied in our transport measurement, since $U_0(H)$ is closely dependent on current density. Different from the Co-free $Ca_{0.82}La_{0.18}FeAs_2$ [47], the values of $U_0(H)$ for $H//ab$ are much larger than that for $H\perp ab$, indicating the intrinsic pinning between the FeAs and CaAs layers is dominant for $H//ab$, and is stronger than the extrinsic pinning due to stacking faults and defects dominant for $H\perp ab$. This result is consistent with many high-T_c su-

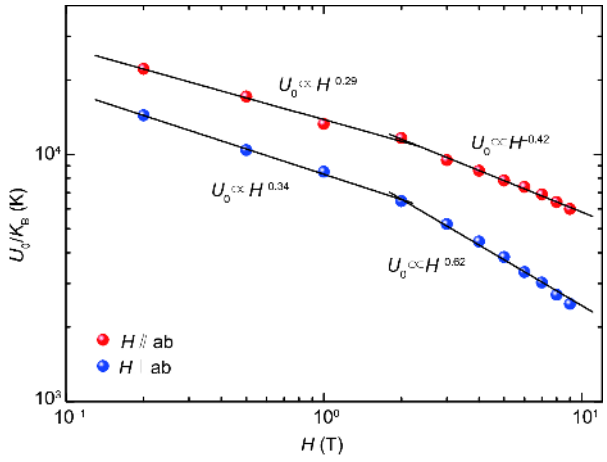

Figure 2 (Color online) Field dependence of U_0 for $Ca_{0.8}La_{0.2}Fe_{0.98}Co_{0.02}As_2$ single crystal (double logarithmic scale). The solid lines indicate the fitting of $U_0 \propto H^{-\alpha}$.

perconductors [9,15,36,48,49]. In addition, for both configurations, it is found that $U_0(H)$ presents two different dependence of magnetic fields, a double linearity in double-logarithmic scale. For $H<2$ T, the $U_0(H)$ values decrease respectively as $H^{-0.29}$ and $H^{-0.34}$ for $H//ab$ and $H\perp ab$, while scale respectively as $H^{-0.42}$ and $H^{-0.62}$ for $H>2$ T, indicating different pinning mechanisms for low and high magnetic fields. Similar crossovers were also observed in other IBSs, e.g., $Ca_{0.82}La_{0.18}FeAs_2$ [47], $SmFeAsO_{0.85}$ [2], Nd(O,F)FeAs [12] and $Fe_{1+y}(Te_{1-x},S_x)_z$ single crystals [36], etc. The weaker field dependence of $U_0(H)$ below 2 T for both configurations indicate that single-vortex pinning is dominant. The vortex spacing becomes significantly smaller than the penetration depth in higher fields and a crossover in a collective-pining regime where the activation energy becomes strongly dependent on the field above 2 T, i.e. the collective creep is dominant [50].

In order to have more insight into the nature of the vortex state in $Ca_{0.8}La_{0.2}Fe_{0.98}Co_{0.02}As_2$, we have analyzed our data using the known vortex-glass theory. According to the vortex-glass theory [51], the resistivity close to the glass transition temperature T_g decreases following the power law:

$$\rho = \rho_0 \left| T / T_g - 1 \right|^s, \tag{3}$$

where ρ_0 is a characteristic resistivity in normal state, and s is a constant related to the various types of disorder. Therefore, T_g can be extracted by applying the Vogel-Fulcher relation to the resistive tail region:

$$(\mathrm{d}\ln\rho / \mathrm{d}T)^{-1} = \left(T - T_g\right) / s. \tag{4}$$

As depicted in Figure 3(a) and (b), T_g, T^* and the critical exponent s are estimated by fitting the linear region of the curves, as indicated by the arrows. The vortex-glass critical temperature, T^*, corresponding to the upper temperature limit of the critical region associated with the vortex-glass to vortex-liquid phase transition, is defined as the temperature which the curve deviates from straight line. The resistivities of $Ca_{0.8}La_{0.2}Fe_{0.98}Co_{0.02}As_2$ single crystal are well described by the vortex-glass picture in a temperature range of $T_g<T<T^*$, symbolizing the presence of the vortex-glass state in $Ca_{0.8}La_{0.2}Fe_{0.98}Co_{0.02}As_2$. Due to the scattering of the data, the values of the exponent s for the different field curves are found to be 3.6±0.2 and 4.7±0.2, for $H\perp ab$ and $H//ab$, respectively. These values are in the range of 2.7-8.5 predicted for the 3D vortex-glass state [44]. Furthermore, according to the modified vortex-glass model [52], the normalized resistivity ρ/ρ_n can be rewritten as:

$$\rho / \rho_n = \left[T\left(T_c - T_g\right) / T_g (T_c - T) - 1 \right]^s. \tag{5}$$

Thus, using the scaled temperature $T_{sc} = [T(T_c - T_g)/T_g(T_c - T) - 1]$, the curves of the normalized resistivity in different magnetic fields should scale into one single curve.

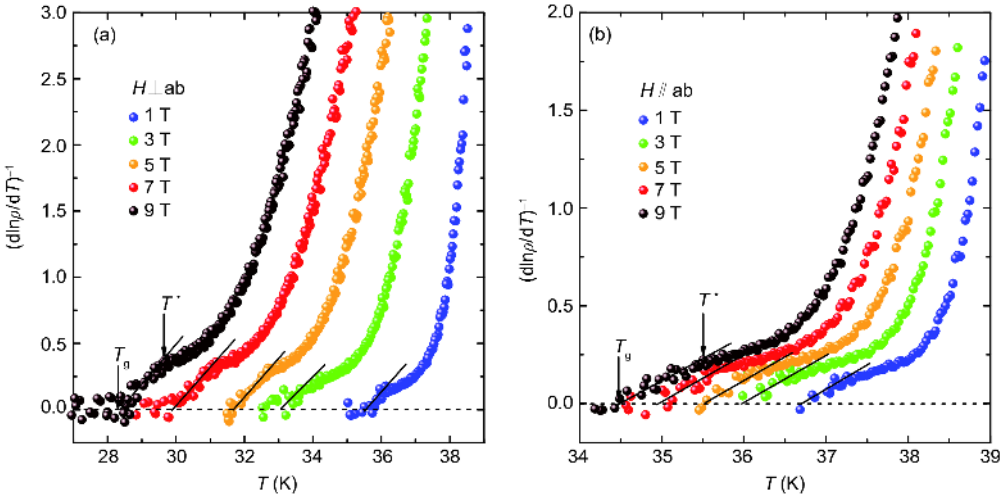

Figure 3 (Color online) Temperature dependence of $[\mathrm{d}(\ln\rho)/\mathrm{d}T]^{-1}$ data at several selective magnetic fields H = 1, 3, 5, 7, and 9 T for (a) $H\perp ab$ and (b) $H//ab$. The vortex glass temperature T_g and critical temperature T^* are estimated based on the linear fitting (see text for detail).

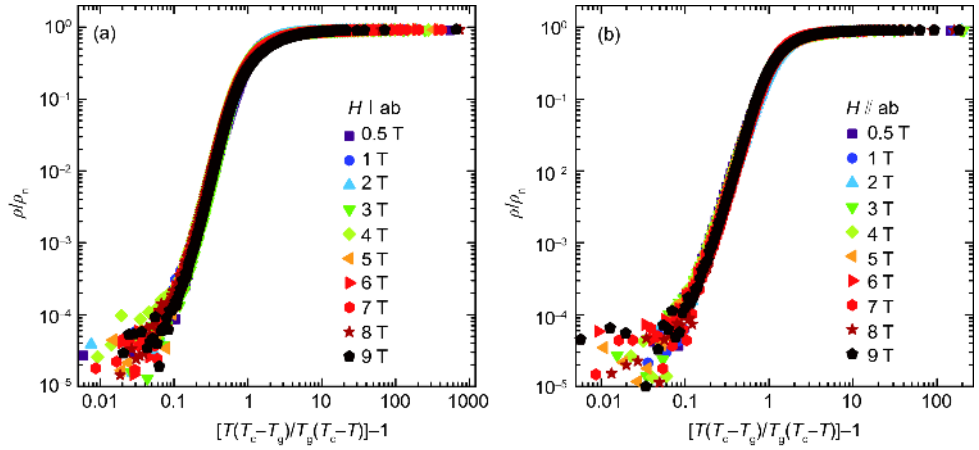

Figure 4 (Color online) The normalized resistivities ρ/ρ_n as a function of scaling temperature T_{sc} in a double log plot for $Ca_{0.8}La_{0.2}Fe_{0.98}Co_{0.02}As_2$ single crystal at various magnetic fields in the cases of (a) $H\perp ab$ and (b) $H//ab$.

Figure 4(a) and (b) depict ρ/ρ_n plotted as a function of T_{sc}, clearly, all data can be well scaled in both directions, further confirming the presence of vortex-glass region in this compound.

Based on the values of T_g and T^* extracted from above analyses, we constructed the static vortex phase diagram of $Ca_{0.8}La_{0.2}Fe_{0.98}Co_{0.02}As_2$ with different dynamic characteristics, as depicted in Figure 5(a) and (b). The upper critical field of H_{c2} is determined from the criterion of the 90%ρ_n. Four different regimes are clearly distinguishable: (1) Vortex-glass state, which governs the region below the vortex-glass line H_g. (2) Vortex-glass critical region, which holds between H_g and H^*, where the vortex lattice becomes softer and melts via a first-order transition into the vortex liquid phase. In this region, resistivity follows the power law as eq. (3). (3) Vortex-liquid phase, the region between the H^* line and the H_{c2} line corresponds to the thorough vortex-liquid behavior. (4) Normal state, the region above H_{c2}.

The Hall effect in the mixed state could provide additional pivotal information on the vortex dynamics. Figure 6(a) and (b) present the field dependence of longitudinal resistivity $\rho_{xx}(H)$ and transverse resistivity $\rho_{xy}(H)$, respectively, from 30 to 40 K with $H\perp ab$. With increasing H, superconductivity is suppressed gradually and the transitions of $\rho_{xx}(H)$ are shifted to lower fields at high temperatures. The Hall resistivity $\rho_{xy}(H)$ (Figure 6(b)) in low fields is zero, and increases in the absolute value at high fields and gradually reaches the $\rho_{xy}(H)$ curve obtained in the normal state at T=40 K, slightly higher than T_c. The negative $\rho_{xy}(H)$ indicates the electron type carriers dominate in the mixed state as well as in the normal state. Moreover, anomalous sign reversal of $\rho_{xy}(H)$ typical for high-T_c cuprates below T_c is not observed [18-21,23-27].

Until now, a variety of theories have been proposed for interpreting the sign reversal, but have not yet given an exhaustive description. It has been suggested, for instance, the appearance of sign reversal is intimately related to the pinning strength, which may induce a backflow of charge carriers and then contribute to the sign reversal [53]. However,

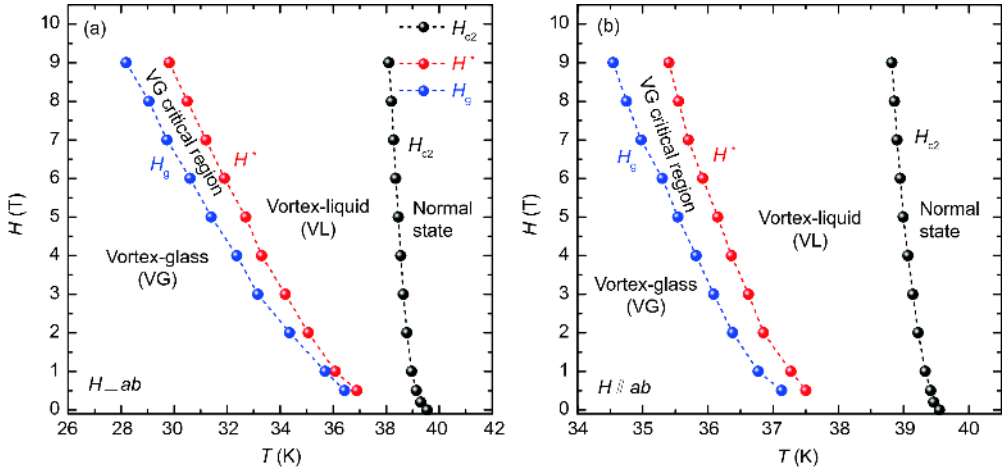

Figure 5 (Color online) Static vortex phase diagram of $Ca_{0.8}La_{0.2}Fe_{0.98}Co_{0.02}As_2$ for (a) $H\perp ab$ and (b) $H//ab$. The upper critical fields H_{c2} are estimated from the criterion of the 90%ρ_n. The characteristic field H_g and H^* are determined from Figure 3. The lines are a guide for eyes.

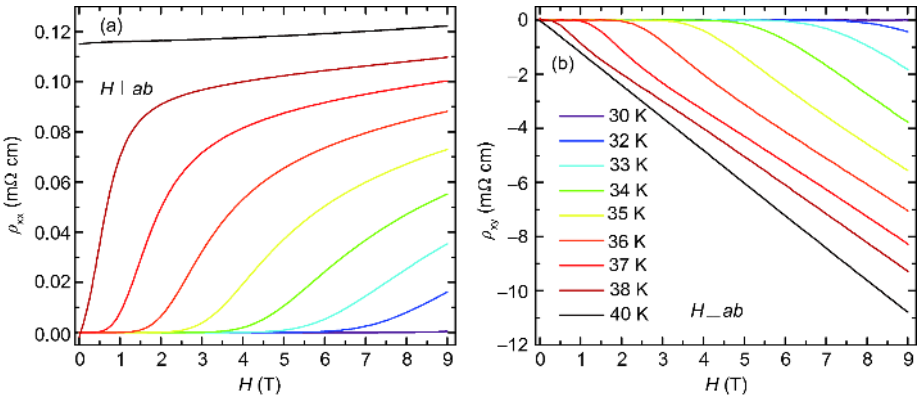

Figure 6 (Color online) Magnetic field dependence of (a) longitudinal resistivity $\rho_{xx}(H)$ and (b) Hall resistivity $\rho_{xy}(H)$ of $Ca_{0.8}La_{0.2}Fe_{0.98}Co_{0.02}As_2$ at various temperatures for $H\perp ab$.

controversial experimental results have been reported on the influence of disorder on the mixed state Hall effect in $YBa_2Cu_3O_{7-\delta}$ single crystal [25]. Additionally, Samoilov et al. [31] and Budhani et al. [21] have also proven that the mixed-state Hall conductivity does not depend on the pinning strength, based on the irradiation experiments in $Tl_2Ba_2Ca_2Cu_3O_{10}$ film, $Tl_2Ba_2CaCu_2O_8$ epitaxial film and $YBa_2Cu_3O_7$ single crystal. In what follows, we would like to analyze the absence of Hall sign reversal in terms of Hall conductivity, $\sigma_{xy}(H)=\rho_{xy}/(\rho_{xy}^2+\rho_{xx}^2)$, which has been pointed out to be independent of disorder by a general argument of the vortex dynamics [21,31,54]. The phenomenological theory based on the time dependent Ginzburg-Landau (TDGL) equation, which does not include the effect of vortex pinning, has been shown to be quite successful in describing the mixed state Hall effect [55,56]. According to the TDGL theory, there are two contributions to the Hall conductivity $\sigma_{xy}(H)$ in the superconducting state:

$$\sigma_{xy}(H) = \sigma_{xy,\mathrm{n}}(H) + \sigma_{xy,\mathrm{sc}}(H). \quad (6)$$

The first term originates from the motion of the quasiparticles inside and around the vortex core. This term has the same sign as the normal state and is proportional to H. The second term is the contribution of the vortex flow and is proportional to $1/H$ [55,56]. Therefore at low magnetic fields, the Hall sign is determined by $\sigma_{xy,\mathrm{sc}}(H)$. The sign reversal can take place if $\sigma_{xy,\mathrm{sc}}(H)$ have a sign opposite to that of $\sigma_{xy,\mathrm{n}}(H)$ below T_c. We replots Figure 6 in terms of $\sigma_{xy}(H)$ as depicted in Figure 7(a). It is clear that $\sigma_{xy}(H)$ tends to diverge to a large negative value and sign reversal is not detected, suggesting that the signs of $\sigma_{xy,\mathrm{n}}(H)$ and $\sigma_{xy,\mathrm{sc}}(H)$ for $Ca_{0.8}La_{0.2}Fe_{0.98}Co_{0.02}As_2$ are the same. In the framework within the BCS theory, several authors have also calculated $\sigma_{xy,\mathrm{sc}}(H)$ and emphasized the importance of the electronic structure of the materials for understanding the Hall effect. For instance, according to the theory proposed by Fukuyama, Ebisawa, and Tsuzuki (FET) [57], the sign of $\sigma_{xy,\mathrm{sc}}(H)$ is determined by the energy derivative $\partial N(0)/\partial\mu$ of the density of states $N(0)$ averaged over the Fermi surface, where μ is the Fermi energy. On the other hand, Aronov, Hikami, and Larkin (AHL) have found that the sign of $\sigma_{xy,\mathrm{sc}}(H)$ is determined by $\partial\ln T_c/\partial\mu$, derived from the Ginsburg-Landau equation and its gauge invariance [58]. In any case, the sign of the Hall effect in the mixed state depends on the details of the band structure. Whereas, Nagaoka et al. [24] have experimentally found that the sign of $\sigma_{xy}(H)$ is universal and is determined by the doping level in cuprates, i.e., a sign reversal occurs in an underdoped regime but diminishes in overdoped ones. This is opposite to what is expected from the predication of the AHL model, suggesting that such model derived from the weak coupling s-wave BCS theory fails to evaluate the hydrodynamic force acting on the vortex of high-T_c cuprates [24,58]. The absence of Hall sign reversal in our study may be consistent with this argument since $Ca_{0.8}La_{0.2}Fe_{0.98}Co_{0.02}As_2$ is located in the overdoped region [59]. However, further studies on both theoretical calculations and experiments are greatly needed to understand the Hall sign reversal, and their relation to the doping level in IBSs.

The scaling behavior of ρ_{xy} between ρ_{xx} for $Ca_{0.8}La_{0.2}Fe_{0.98}Co_{0.02}As_2$ single crystal is plotted in Figure 7(b). It is evident that ρ_{xy} and ρ_{xx} follow the relation $|(\rho_{xy}(H)|=A\rho_{xx}(H)^{\beta}$ very well and the β values are close to 2 as shown in the inset. Various β values have been found in several types of high-T_c superconductors, such as YBCO single crystals (β~1.7) [30], BSCCO (β~2) [32] and TBCCO (β~2) [20, 21] in cuprates, and Fe(Te,S) (β=0.9-1.0) [36], $Ba(Fe_{1-x}Co_x)As_2$ (β=2.0-3.4) [33] and $Li_x(NH_3)_yFe_2Se_2$ (β~2.0) [9] in IBSs. The Hall scaling behavior is a complicated phenomenon, many efforts, both theoretical and experimental, have been made to account for it. The first theoretical attempt was presented by Dorsey and Fisher [60], who developed a scaling theory with an exponent β=1.7 in the framework of glassy scaling near a vortex-glass transition, and explained the experimental results of Luo et al. [30] for YBCO films. A phenomenological model was put forward afterwards by Vinokur et al. [54],

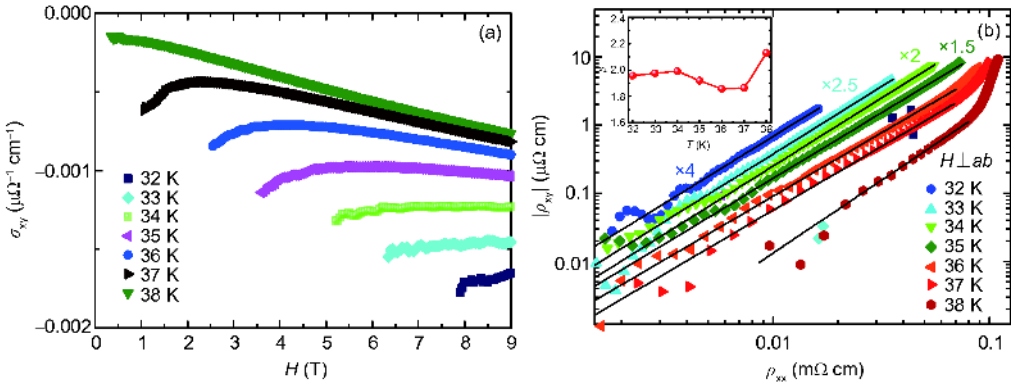

Figure 7 (Color online) (a) Field dependence of the Hall conductivity $\sigma_{xy}(H)=\rho_{xy}/(\rho_{xy}^2+\rho_{xx}^2)$ measured at various temperatures. (b) Scaling behavior between $|\rho_{xy}|$ and ρ_{xx} at various temperatures for $Ca_{0.8}La_{0.2}Fe_{0.98}Co_{0.02}As_2$. Solid lines are fitting results using the relation $|(\rho_{xy}(H)|=A\rho_{xx}(H)^{\beta}$. Curves for below 35 K are shifted along the vertical axis for the sake of clarity. Inset: temperature dependence of $\beta(T)$.

who suggested that the scaling behavior with an exponent β=2 is believed to be a general feature in the flux-flow region and independent of the pinning strength. This model was strongly supported by the experimental results [31,32]. Another phenomenological model was proposed by Wang, Dong and Ting (WDT) [53], who claimed that β could change from 2 to 1.5 as the pinning strength increased, which agreed with the results reported for YBCO crystals [61] and Hg-1212 films [62]. Nevertheless, this theory seems to fail in explaining all the scaling behavior of high-T_c superconductors. For instance, no influence of disorder on the scaling exponent have confirmed in TBCCO film and YBCO single crystal irradiated via heavy ions [21,31]. A similar case was also found in MgB_2 films, which follows a universal Hall scaling behavior with a constant exponent β of 2±0.1 and is independent of the pinning strength [63]. The above controversial experimental and theoretical results indicate the scaling behavior in the mixed state is not yet fully understood, especially whether or not the pinning effect plays an important role on it. Herein, for $Ca_{0.8}La_{0.2}Fe_{0.98}Co_{0.02}As_2$ single crystal, the appearance of the second magnetization peak, critical current density and large values of activation energy U_0 imply relatively strong pinning in this compound [6]. Considering the above-mentioned theories, our experiment result (β~2) seems to be in agreement with the theory proposed by Vinokur et al. [54], but is inconsistent with the WDT theory in which claims the scaling behavior is closely related to the pinning strength, i.e. a β value less than 2 is generally expected to be in the strong pinning case [9,35,53]. However, more work is necessary for better understanding of the scaling law and the influence of pinning strength on it in the future.

4 Conclusion

To summarize, we have studied the transport properties in the superconducting mixed state of $Ca_{0.8}La_{0.2}Fe_{0.98}Co_{0.02}As_2$ single crystal. The magnetic field dependence of the activation energy, which is derived in the framework of TAFF theory, shows double-linear field dependence in both field directions, i.e. weak power law decrease of $U_0(H)$ in low fields and more rapidly decrease of $U_0(H)$ in high fields, respectively, signifying a transition from single vortex pinning to collective creep pinning with increasing field. Meanwhile, vortex-glass to vortex-liquid state transition was detected based on the vortex-glass theory, and the static vortex phase diagram was also depicted. Besides these, the mixed-state Hall effect indicates that there is no sign reversal. Also, the scaling behavior $|(\rho_{xy}(H)|=A\rho_{xx}(H)^{\beta}$ with the scaling exponent β~2.0 in the relative strong pinning $Ca_{0.8}La_{0.2}Fe_{0.98}Co_{0.02}As_2$, in accordance with many previous reports on high-T_c cuprates and MgB_2, possibly coincide with the phenomenological theory which suggested the scaling behavior to be independent of the pinning strength. Our results provide new insight into future theoretical and experimental studies on the vortex motion in the mixed state of IBSs.

The authors thank Prof. HaiHu Wen and Prof. DingPing Li for helpful discussions. This work was supported by the National Natural Science Foundation of China (Grant Nos. 11674054, and 11611140101). XiangZhou Xing was also sponsored by the Scientific Research Foundation of Graduate School of Southeast University (Grant No. YBJJ1621).

1 Y. Kamihara, T. Watanabe, M. Hirano, and H. Hosono, J. Am. Chem. Soc. **130**, 3296 (2008).
2 H. S. Lee, M. Bartkowiak, J. S. Kim, and H. J. Lee, Phys. Rev. B **82**, 104523 (2010).
3 R. Prozorov, N. Ni, M. A. Tanatar, V. G. Kogan, R. T. Gordon, C. Martin, E. C. Blomberg, P. Prommapan, J. Q. Yan, S. L. Bud'Ko, and P. C. Canfield, Phys. Rev. B **78**, 224506 (2008), arXiv: 0810.1338.
4 S. R. Ghorbani, X. L. Wang, M. Shabazi, S. X. Dou, K. Y. Choi, and C. T. Lin, Appl. Phys. Lett. **100**, 072603 (2012).
5 Y. Sun, S. Pyon, T. Tamegai, R. Kobayashi, T. Watashige, S. Kasahara, Y. Matsuda, and T. Shibauchi, Phys. Rev. B **92**, 144509 (2015), arXiv:

1510.05753.
6 W. Zhou, X. Xing, W. Wu, H. Zhao, and Z. Shi, Sci. Rep. **6**, 22278 (2016).
7 B. Shen, P. Cheng, Z. Wang, L. Fang, C. Ren, L. Shan, and H. H. Wen, Phys. Rev. B **81**, 014503 (2010), arXiv: 0910.3600.
8 S. Salem-Sugui Jr., L. Ghivelder, A. D. Alvarenga, L. F. Cohen, K. A. Yates, K. Morrison, J. L. Pimentel Jr., H. Luo, Z. Wang, and H. H. Wen, Phys. Rev. B **82**, 054513 (2010), arXiv: 1008.2880.
9 S. Sun, S. Wang, C. Li, and H. Lei, Supercond. Sci. Technol. **31**, 015003 (2018), arXiv: 1705.08810.
10 X. Yi, C. Wang, Q. Tang, T. Peng, Y. Qiu, J. Xu, H. Sun, Y. Luo, and B. Yu, Supercond. Sci. Technol. **29**, 105015 (2016).
11 L. Jiao, Y. Kohama, J. L. Zhang, H. D. Wang, B. Maiorov, F. F. Balakirev, Y. Chen, L. N. Wang, T. Shang, M. H. Fang, and H. Q. Yuan, Phys. Rev. B **85**, 064513 (2012), arXiv: 1106.2283.
12 J. Jaroszynski, F. Hunte, L. Balicas, Y. Jo, I. Raičević, A. Gurevich, D. C. Larbalestier, F. F. Balakirev, L. Fang, P. Cheng, Y. Jia, and H. H. Wen, Phys. Rev. B **78**, 174523 (2008), arXiv: 0810.2469.
13 G. Prando, P. Carretta, R. de Renzi, S. Sanna, A. Palenzona, M. Putti, and M. Tropeano, Phys. Rev. B **83**, 174514 (2011), arXiv: 1102.1404.
14 S. Salem-Sugui Jr., J. Mosqueira, A. D. Alvarenga, D. Sóñora, A. Crisan, A. M. Ionescu, S. Sundar, D. Hu, S. L. Li, and H. Q. Luo, Supercond. Sci. Technol. **30**, 055003 (2017).
15 J. C. Lu, Y. Yu, L. Pi, and Y. H. Zhang, Chin. Phys. B **23**, 127402 (2014).
16 M. Andersson, A. Rydh, and Ö. Rapp, Phys. Rev. B **63**, 184511 (2001).
17 B. D. Josephson, Phys. Lett. **16**, 242 (1965).
18 S. J. Hagen, A. W. Smith, M. Rajeswari, J. L. Peng, Z. Y. Li, R. L. Greene, S. N. Mao, X. X. Xi, S. Bhattacharya, Q. Li, and C. J. Lobb, Phys. Rev. B **47**, 1064 (1993).
19 V. N. Narozhnyi, J. Freudenberger, V. N. Kochetkov, K. A. Nenkov, G. Fuchs, A. Handstein, and K. H. Müller, Phys. Rev. B **59**, 14762 (1999).
20 A. V. Samoilov, Z. G. Ivanov, and L. G. Johansson, Phys. Rev. B **49**, 3667 (1994).
21 R. C. Budhani, S. H. Liou, and Z. X. Cai, Phys. Rev. Lett. **71**, 621 (1993).
22 S. Bhattacharya, M. J. Higgins, and T. V. Ramakrishnan, Phys. Rev. Lett. **73**, 1699 (1994).
23 Y. Matsuda, T. Nagaoka, G. Suzuki, K. Kumagai, M. Suzuki, M. Machida, M. Sera, M. Hiroi, and N. Kobayashi, Phys. Rev. B **52**, R15749 (1995).
24 T. Nagaoka, Y. Matsuda, H. Obara, A. Sawa, T. Terashima, I. Chong, M. Takano, and M. Suzuki, Phys. Rev. Lett. **80**, 3594 (1998).
25 R. Jin, and H. R. Ott, Phys. Rev. B **57**, 13872 (1998).
26 L. M. Wang, H. C. Yang, and H. E. Horng, Phys. Rev. Lett. **78**, 527 (1997).
27 Z. Wang, Y. Z. Zhang, X. F. Lu, H. Gao, L. Shan, and H. H. Wen, Physica C **422**, 41 (2005).
28 J. Bardeen, and M. J. Stephen, Phys. Rev. **140**, A1197 (1965).
29 P. Nozières, and W. F. Vinen, Philos. Mag. **14**, 667 (1966).
30 J. Luo, T. P. Orlando, J. M. Graybeal, X. D. Wu, and R. Muenchausen, Phys. Rev. Lett. **68**, 690 (1992).
31 A. V. Samoilov, A. Legris, F. Rullier-Albenque, P. Lejay, S. Bouffard, Z. G. Ivanov, and L. G. Johansson, Phys. Rev. Lett. **74**, 2351 (1995).
32 A. V. Samoilov, Phys. Rev. Lett. **71**, 617 (1993).
33 L. M. Wang, U. C. Sou, H. C. Yang, L. J. Chang, C. M. Cheng, K. D. Tsuei, Y. Su, T. Wolf, and P. Adelmann, Phys. Rev. B **83**, 134506 (2011).
34 H. Sato, T. Katase, W. N. Kang, H. Hiramatsu, T. Kamiya, and H. Hosono, Phys. Rev. B **87**, 064504 (2013), arXiv: 1302.3696.
35 L. M. Wang, C. Y. Wang, U. C. Sou, H. C. Yang, L. J. Chang, C. Redding, Y. Song, P. Dai, and C. Zhang, J. Phys.-Condens. Matter **25**, 395702 (2013).
36 H. Lei, R. Hu, E. S. Choi, and C. Petrovic, Phys. Rev. B **82**, 134525 (2010), arXiv: 1010.0263.
37 N. Katayama, K. Kudo, S. Onari, T. Mizukami, K. Sugawara, Y. Sugiyama, Y. Kitahama, K. Iba, K. Fujimura, N. Nishimoto, M. Nohara, and H. Sawa, J. Phys. Soc. Jpn. **82**, 123702 (2013), arXiv: 1311.1303.
38 X. Xing, W. Zhou, N. Zhou, F. Yuan, Y. Pan, H. Zhao, X. Xu, and Z. Shi, Supercond. Sci. Technol. **29**, 055005 (2016), arXiv: 1603.05392.
39 X. Xing, W. Zhou, J. Wang, Z. Zhu, Y. Zhang, N. Zhou, B. Qian, X. Xu, and Z. Shi, Sci. Rep. **7**, 45943 (2017).
40 H. Yakita, H. Ogino, T. Okada, A. Yamamoto, K. Kishio, T. Tohei, Y. Ikuhara, Y. Gotoh, H. Fujihisa, K. Kataoka, H. Eisaki, and J. Shimoyama, J. Am. Chem. Soc. **136**, 846 (2014).
41 X. Xing, W. Zhou, B. Xu, N. Li, Y. Sun, Y. Zhang, and Z. Shi, J. Phys. Soc. Jpn. **84**, 075001 (2015).
42 J. Deak, M. McElfresh, D. W. Face, and W. L. Holstein, Phys. Rev. B **52**, R3880 (1995).
43 W. K. Kwok, S. Fleshler, U. Welp, V. M. Vinokur, J. Downey, G. W. Crabtree, and M. M. Miller, Phys. Rev. Lett. **69**, 3370 (1992).
44 G. Blatter, M. V. Feigel'Man, V. B. Geshkenbein, A. I. Larkin, and V. M. Vinokur, Rev. Mod. Phys. **66**, 1125 (1994).
45 T. T. M. Palstra, B. Batlogg, L. F. Schneemeyer, and J. V. Waszczak, Phys. Rev. Lett. **61**, 1662 (1988).
46 T. T. M. Palstra, B. Batlogg, R. B. van Dover, L. F. Schneemeyer, and J. V. Waszczak, Phys. Rev. B **41**, 6621 (1990).
47 W. Zhou, J. Zhuang, F. Yuan, X. Li, X. Xing, Y. Sun, and Z. Shi, Appl. Phys. Express **7**, 063102 (2014), arXiv: 1405.6558.
48 D. Ahmad, W. J. Choi, Y. I. Seo, S. Seo, S. Lee, and Y. S. Kwon, Results Phys. **7**, 16 (2017).
49 X. L. Wang, S. R. Ghorbani, S. I. Lee, S. X. Dou, C. T. Lin, T. H. Johansen, K. H. Müller, Z. X. Cheng, G. Peleckis, M. Shabazi, A. J. Qviller, V. V. Yurchenko, G. L. Sun, and D. L. Sun, Phys. Rev. B **82**, 024525 (2010), arXiv: 1002.2095.
50 Y. Yeshurun, and A. P. Malozemoff, Phys. Rev. Lett. **60**, 2202 (1988).
51 D. S. Fisher, M. P. A. Fisher, and D. A. Huse, Phys. Rev. B **43**, 130 (1991).
52 A. Rydh, Ö. Rapp, and M. Andersson, Phys. Rev. Lett. **83**, 1850 (1999).
53 Z. D. Wang, J. Dong, and C. S. Ting, Phys. Rev. Lett. **72**, 3875 (1994).
54 V. M. Vinokur, V. B. Geshkenbein, M. V. Feigel'man, and G. Blatter, Phys. Rev. Lett. **71**, 1242 (1993).
55 N. B. Kopnin, B. I. Ivlev, and V. A. Kalatsky, J. Low Temp. Phys. **90**, 1 (1993).
56 A. T. Dorsey, Phys. Rev. B **46**, 8376 (1992).
57 H. Fukuyama, H. Ebisawa, and T. Tsuzuki, Prog. Theor. Phys. **46**, 1028 (1971).
58 A. G. Aronov, S. Hikami, and A. I. Larkin, Phys. Rev. B **51**, 3880 (1995).
59 W. Zhou, F. Ke, X. Xu, R. Sankar, X. Xing, C. Q. Xu, X. F. Jiang, B. Qian, N. Zhou, Y. Zhang, M. Xu, B. Li, B. Chen, and Z. X. Shi, Phys. Rev. B **96**, 184503 (2017).
60 A. T. Dorsey, and M. P. A. Fisher, Phys. Rev. Lett. **68**, 694 (1992).
61 W. N. Kang, D. H. Kim, S. Y. Shim, J. H. Park, T. S. Hahn, S. S. Choi, W. C. Lee, J. D. Hettinger, K. E. Gray, and B. Glagola, Phys. Rev. Lett. **76**, 2993 (1996).
62 W. N. Kang, S. H. Yun, J. Z. Wu, and D. H. Kim, Phys. Rev. B **55**, 621 (1997).
63 W. N. Kang, H. J. Kim, E. M. Choi, H. J. Kim, K. H. P. Kim, and S. I. Lee, Phys. Rev. B **65**, 184520 (2002).